Sensors & Actuators: B. Chemical 302 (2020) 127205

Contents lists available at ScienceDirect

Sensors and Actuators B: Chemical

journal homepage: www.elsevier.com/locate/snb

# YSZ-based solid electrolyte type sensor utilizing $ZnMoO_4$ sensing electrode for fast detection of ppb-level $H_2S$

Fangmeng Liu[a,*], Jing Wang[a], Rui You[b], Zijie Yang[a], Junming He[a], Caileng Wang[a], Ao Liu[a], Qingji Wang[c], Xu Yan[a], Peng Sun[a], Geyu Lu[a,*]

[a] State Key Laboratory of Integrated Optoelectronics, Key Laboratory of Advanced Gas Sensors, Jilin Province, College of Electronic Science and Engineering, Jilin University, 2699 Qianjin Street, Changchun 130012, China
[b] Institute of Microelectronics, Peking University, Beijing, 100871, China
[c] State Key Laboratory of Marine Resource Utilization in South China Sea, Hainan University, Haikou 570228, PR China

ARTICLE INFO

*Keywords:*
$H_2S$ sensor
Stabilized zirconia
Mixed-potential
$ZnMoO_4$
Ppb-level

ABSTRACT

The planar and compact type all-solid state electrochemical gas sensing device based on yttria-stabilized zirconia (YSZ) and Zinc molybdate ($ZnMoO_4$) composite sensing electrode (SE) was proposed and fabricated to effectively detect ppb-level $H_2S$ at high temperature. The gas sensing property of different SEs ($ZnMoO_4$, $CoMoO_4$ and $NiMoO_4$) is compared and explored. The sensor attached with $ZnMoO_4$-SE processes the highest response value of −62.5 mV to 1 ppm $H_2S$ and lower detection limit of 5 ppb $H_2S$ at 500 °C. The response and recovery times of the sensor to 500 ppb $H_2S$ are 20 s and 58 s, respectively. The sensor also displays high sensitivity, good continuous reproducibility, selectivity and stability of humidity and high temperature at 500 °C. In addition, the sensing principle involving mixed potential model was proposed and verified using polarization curves.

## 1. Introduction

Hydrogen sulfide ($H_2S$) is a kind of nerve agent and is also an extremely choking and irritating gas with a rotten eggs smell. After releasing into the atmosphere, it will cause serious harm to the surrounding environment and human life and health. The key sources of $H_2S$ are mainly concentrated on the exhaust gas emitted by natural gas plants, chemical plants, water and gas plants and smelters [1]. Therefore, presently how to *in-situ* monitor $H_2S$ in flue gas has become a very important issue using simple, miniaturized, and low cost gas detection device at high temperature, and also has very important economic benefits and social significance.

To date, numerous research efforts have been mostly focused on development and fabrication of $H_2S$ gas sensor with simple manufacture process, inexpensive cost, excellent sensitivity and rapid response speed based on different functional materials, such as metal oxide semiconductor [2–10], solid electrolytes [11–13], organic material [14,15], MOF [16,17] and so on. Among the multitudinous developed $H_2S$ gas sensors, the solid electrolyte type electrochemical sensing devices have played an enormous potential in detection of low concentration $H_2S$. Yang et al fabricated a room temperature fuel cell type amperometric $H_2S$ sensor using proton exchange membrane (Nafion) and Pt-Rh nanoparticles loaded carbon fibers sensing electrode for detection of 0.1–200 ppm $H_2S$ [12]. Zhang et al. used spinel-type oxide $CoCr_{2-x}Mn_xO_4$ as sensing electrode to fabricate sodium super ionic conductor (NASICON)-based solid electrochemical sub-ppm $H_2S$ sensor, which exhibits excellent selectivity at 250 °C [18]. Although above-mentioned solid electrolyte type sensor showed satisfactory sensing characteristics, the shortcoming for operating at low temperature is insuperable. Fortunately, the stabilized zirconia-based mixed potential type $H_2S$ sensors using different metal oxide sensing electrodes are got high expectations due to the stable ability of high temperature, high humidity and various gas coexistence. Miura et al. designed a tube type of electrochemical mixed potential type $H_2S$ sensor combining yttria-stabilized zirconia with $WO_3$ sensing electrode, which was found to respond well to 0.2–25 ppm $H_2S$ at 400 °C [13]. Lu et al fabricated the mixed potential type sub-ppm $H_2S$ sensor based on YSZ and hollow balls $NiMn_2O_4$ sensing electrode, and the sensing device exhibited the low detection limit of 50 ppb and excellent selectivity at 500 °C [19]. Subsequently, a $K_2NiF_4$-type $La_2NiO_4$ as sensing electrode was first fabricated YSZ-based mixed potential type $H_2S$ sensor. The recovery time of the sensor to 500 ppb $H_2S$ was about 150 s at 500 °C [20]. However, the response/recovery time, the detection limit, selectivity and sensitivity for YSZ-based $H_2S$ sensor based on the mixed potential principle still have much space to improve by designing novel sensing electrode material.

* Corresponding authors.
*E-mail addresses:* liufangmeng@jlu.edu.cn (F. Liu), lugy@jlu.edu.cn (G. Lu).

https://doi.org/10.1016/j.snb.2019.127205
Received 18 May 2019; Received in revised form 14 August 2019; Accepted 27 September 2019
Available online 27 September 2019
0925-4005/ 

Bimetal oxide material systems with multiple-functionalities and prominent electrochemical catalytic activity, selectivity, and stability attracts increasing interest in the design of new materials for gas sensing device. Recently metal molybdates $MMoO_4$ have been investigated and tried to applied in humidity sensing, photo/electrocatalytic, and electrochemical energy storage etc. However, for the development of stabilized zirconia-based solid electrolyte type gas sensor, metal molybdates as sensing electrode is rarely reported. Its potential as sensing electrode material for YSZ-based $H_2S$ gas sensor is anticipated. Moreover, achieving bimetal molybdates ($ZnMoO_4$, $CoMoO_4$ and $NiMoO_4$) as sensing electrodes on the basis of developed single metal oxides (include $Ni^{2+}$, $Co^{2+}$ and $Zn^{2+}$ as metal element) of YSZ-based gas sensor is an important choice to fabricate high performance sensing device. In this work, a new mixed potential type stabilized zirconia-based gas sensor utilizing molybdate $MMoO_4$ ($ZnMoO_4$, $CoMoO_4$ and $NiMoO_4$) composite oxides sensing electrodes was first presented and fabricated for fast detection of ppb-level $H_2S$ at 500 °C. The sensing device attached with $ZnMoO_4$-SE exhibited fast response and recovery times of 20 s and 58 s to 500 ppb $H_2S$ and low detection limit of 5 ppb at 500 °C. Furthermore, the gas-sensing performance and sensing mechanism was also systematically investigated and discussed.

## 2. Experimental

Herein, three metal molybdate $MMoO_4$ ($ZnMoO_4$, $CoMoO_4$ and $NiMoO_4$) sensing materials were designed and selected as sensing electrodes of YSZ-based solid electrolyte type $H_2S$ gas sensor, respectively. The plate YSZ substrate (8 mol% $Y_2O_3$-stabilized $ZrO_2$, 2 mm × 2 mm × 0.3 mm of length × width × thickness, purchased from Anpeisheng Corp., China) was used as solid electrolyte. The Zinc molybdate ($ZnMoO_4$) sensing electrode material was synthesized from $Zn(Ac)_2{\cdot}2H_2O$ and $Na_2MoO_4{\cdot}2H_2O$ according to Reference [21]. Subsequently, the as-synthesized precursor was calcinated in muffle furnace at 800 °C for 2 h. $CoMoO_4$ and $NiMoO_4$ sensing materials were also calcinated at same condition. Fig. 1 illustrates the schematic diagram of the fabricated sensor and the detailed fabrication process as follows. Originally, both left and right ends of YSZ-substrate were printed by point-shaped and stripe-shaped Pt (provided by Sino-platinum Metals Co., Ltd.), respectively. Meanwhile, Pt wire (Diameter of 0.02 mm, purchasing from Sino-platinum Metals Co., Ltd.) was attached to Pt point and Pt stripe as the signal collection leads. The above-obtained substrate was sintered at 1000 °C for 0.5 h to get Pt reference electrode (RE) at the end of stripe-shape Pt. Then, three molybdate ($ZnMoO_4$, $CoMoO_4$ and $NiMoO_4$) sensing materials were mixed with a minimum quantity of deionized water to get sensing electrode pastes, respectively. The stripe-shaped sensing electrode (SE) was formed on the point-shaped Pt using a fine brush. To gain good contact between the sensing electrode and YSZ electrolyte, the device was calcinated for 2 h at 800 °C. Whereafter, the $Al_2O_3$ substrate with Pt heater (length × width × thickness: 2 mm × 2 mm × 0.2 mm, providing the working temperature for the sensing device) was adhered to the back of YSZ substrate by the inorganic adhesive (formed by preparation of sodium silicate and alumina powder) to get sensitive unit. Finally, above sensitive unit was welded to the hexagon socket to obtain integral structural gas sensor. The above-fabricated sensing device was connected to a digital electrometer (Rigol. DM3054) and the potential difference signal between SE and RE was measured and investigated in various tested gases or air based on static state test system. The polarization curves of sensor were carried out utilizing the electrochemical workstation (CHI600C, Instrument corporation of Shanghai, China) in air and different concentrations of $H_2S$ gas (0.5 ppm and 1 ppm $H_2S$ + air) at 500 °C.

The crystallinity and phase information of $ZnMoO_4$ composite were structurally characterized by X-ray diffraction (XRD) patterns utilizing Rigaku wide-angle X-ray diffractometer (D/max rA, Cu Kα radiation at wave length = 0.1541 nm). Raman spectroscopy of $ZnMoO_4$ sensing material was operated on LabRAM HR Evolution spectrometer with a laser wavelength of 532 nm. The surface morphology and microstructure of $ZnMoO_4$-SE was recorded using field-emission scanning electron microscopy (FESEM, JEOL JSM-7500 F, with an accelerating voltage of 5 kV). X-ray photoelectron spectroscopy (XPS) was performed using a Thermo ESCALAB250 spectrometer equipped with an Al-Kα ray source to obtain the composition information of $ZnMoO_4$.

## 3. Results and discussion

Fig. 2**(a)** illustrated XRD pattern of the $ZnMoO_4$ sensing material annealed at 800 °C. All XRD diffraction peaks can be indexed perfectly

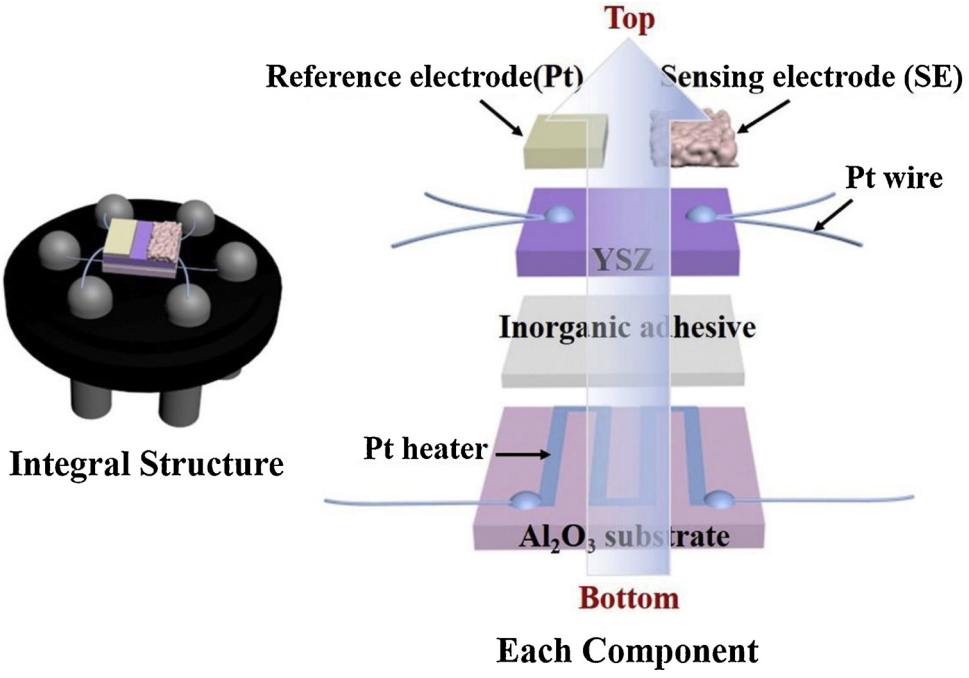


**Fig. 1.** Schematic diagram of fabricated sensor.

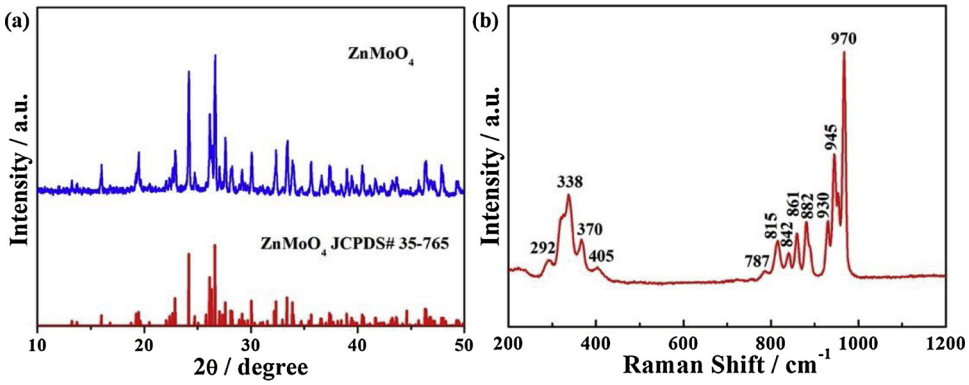


**Fig. 2.** (a) XRD pattern and (b) of Raman spectrum $ZnMoO_4$ sensing material calcinated at 800 °C.

to triclinic structured $ZnMoO_4$ with space group P1 (JCPDS 35–765) [22]. No diffraction peaks of any other impurity are observed, confirming the formation of single-phase of alpha-$ZnMoO_4$. The sharp diffraction peaks for composite oxide material annealed at 800 °C revealed good crystalline nature. In order to further identify the chemical structure information, Raman spectroscopy of sensing material was measured, as shown in Fig. 2**(b)**. Normally, the symmetric stretching vibration modes (υ1) and asymmetric stretching vibration modes (υ3) of $MoO_4$ tetrahedra for $ZnMoO_4$ are recorded in the range of 700-1000 $cm^{-1}$. Raman bands corresponding to symmetric bending vibration modes (υ2) and asymmetric bending vibration modes (υ4) of $MoO_4$ tetrahedra are observed in the region of 300-520 $cm^{-1}$ [23–25]. Consequently, the Raman peaks observed at 787 $cm^{-1}$, 815 $cm^{-1}$, 842 $cm^{-1}$, 861 $cm^{-1}$ and 880 $cm^{-1}$ can be assigned to asymmetric stretching vibration modes of $MoO_4$ tetrahedra. And the Raman band observed at 930 $cm^{-1}$, 945 $cm^{-1}$ and 970 $cm^{-1}$ may result from a symmetric stretching vibration in $MoO_4$ tetrahedral units. The Raman band at 338 $cm^{-1}$ can be assigned to the symmetric bending vibration (υ2) or asymmetric bending vibration (υ4) of $ZnMoO_4$.

The morphology of $ZnMoO_4$-SE sintered at 800 °C is exhibited in Fig. 3**(a)**. $ZnMoO_4$ sensing electrode material sintered at 800 °C is composed of conjoined particle with diameter of micro-scale. The sensing electrode possess of loose and porous structure, which provides smooth gas diffusion path in sensing electrode layer. Furthermore, to further corroborates the observed result of XRD and Raman, XPS was performed to study the elemental composition and oxidation state of $ZnMoO_4$. As shown in Fig. 3**(b)**, Zn, Mo, O and C elements are existed in the survey of $ZnMoO_4$. The Zn 2p region shows two binding energy peaks at 1045.6 and 1022.6 eV, attributing to Zn $2p_{1/2}$ and Zn $2p_{3/2}$, respectively. The energy separation of 23.0 eV between Zn $2p_{1/2}$ and Zn $2p_{3/2}$ demonstrates the characteristic of $Zn^{2+}$ in $ZnMoO_4$ (Fig. 3**(d)**) [26]. The binding energy and calculated splitting width (3.2 eV) between $Mo3d_{5/2}$ and $Mo3d_{3/2}$ are in good agreement with $Mo^{6+}$ (Fig. 3**(d)**) [27].

For the mixed potential type YSZ-based gas sensing device, the sensing electrode material category is acknowledged to be pivotal in sensing property of the sensor. Herein, three molybdate sensing materials ($MMoO_4$ (M: Co, Ni and Zn)) were applied to fabricate planar type YSZ solid electrolyte device, aiming at optimizing detection ability of $H_2S$. As depicted in Fig. 4, the sensor using $ZnMoO_4$-SE sintered at

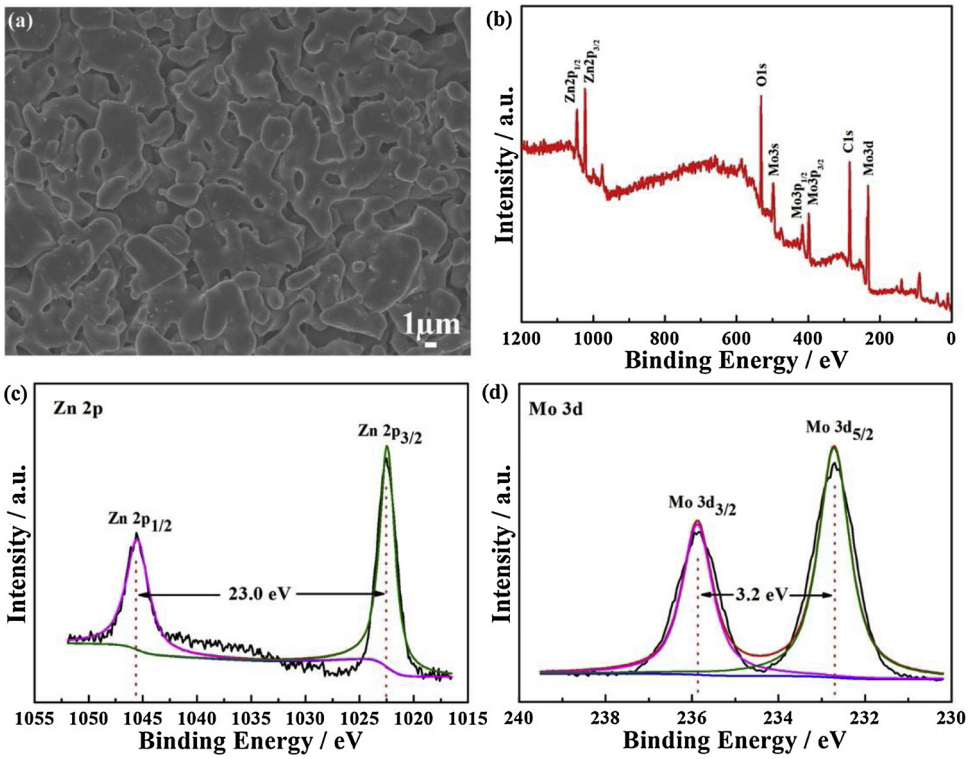


**Fig. 3.** (a) SEM image of $ZnMoO_4$-SE; XPS spectra of $ZnMoO_4$ sintered at 800 °C (b) survey; (c) Zn 2p and (d) Mo 3d.

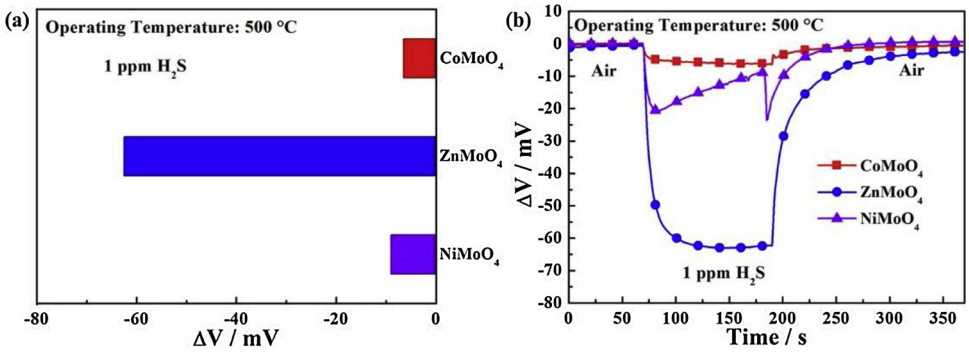


**Fig. 4.** (a) Comparation of the response value for the sensor using $MMoO_4$ (M: Co, Ni and Zn) sintered at 800 °C to 1 ppm $H_2S$ at 500 °C; (b) Response and recovery curves of the sensors to 1 ppm $H_2S$ at 500 °C.

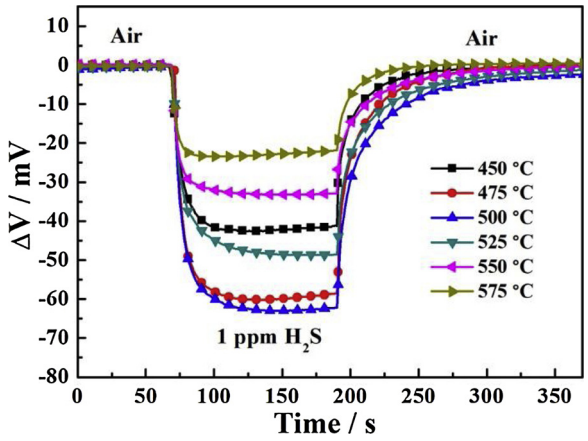


**Fig. 5.** Response transients of the sensor utilizing $ZnMoO_4$-SE sintered at 800 °C to 1 ppm $H_2S$ at different working temperatures.

800 °C possessed the highest response value to 1 ppm $H_2S$ at 500 °C compared with devices attached with $CoMoO_4$-SE and $NiMoO_4$-SE, which reveals tremendous potential in effective detection of $H_2S$. Accordingly, the present main work concentrates on the investigation and evaluation of sensing performances for the sensor utilizing $ZnMoO_4$-SE. As reported in literatures [28–30], the working temperature of the device greatly determined the sensing property due to effect of adsorption/desorption and activation energy. Consequently, the response transients of the sensor utilizing $ZnMoO_4$-SE sintered at 800 °C to 1 ppm $H_2S$ at different working temperatures are measured and shown in Fig. 5. Explicitly, in the working temperature range of 450–575 °C, the fabricated sensor appears in the trend of first increased then decreased to 1 ppm $H_2S$ and the best sensing property is achieved at 500 °C. At low working temperature (< 500 °C), the activation energy for electrochemical reaction is slightly deficiency, leading to a poor response. With increasing the working temperature, the electrochemical reaction at TPB (Triple Phase Boundary, the interface of $ZnMoO_4$, YSZ and $H_2S$) will quickly enhance, leading to improved response. While further increasing the working temperature, the desorption process of $H_2S$ proceeds dominant following the adsorption amount of $H_2S$ decrease, which results in deterioration of response at higher temperature. Therefore, the optimal operating temperature of 500 °C for the sensor utilizing $ZnMoO_4$-SE sintered at 800 °C is chosen in the following study.

Fig. 6**(a)** shows response transients of the sensor using $ZnMoO_4$-SE sintered at 800 °C to 0.005–5 ppm $H_2S$ at 500 °C. To guarantee the consistence and uniformity of response transients, the same measurement time of about 2 min in different concentration of $H_2S$ and the consistent test time of 3 min in air are used. And the response potential signal value at last second in $H_2S$ gas was used as the potential value for the calibration curves. Evidently, when the sensor is exposed to $H_2S$ atmosphere, the response signal of the device attached with $ZnMoO_4$-SE sintered at 800 °C exhibited negative change and gradually increased in negative direction with increase of $H_2S$ concentrations in the ranges of 0.005–5 ppm. It is noticeable that the response value to 0.1 ppm and 1 ppm $H_2S$ is −13 mV and −62.6 mV, the lowest detection limit can even be approach to 5 ppb $H_2S$ at response signal of −3.2 mV. Furthermore, the sensor possessed good response and recovery characteristics to $H_2S$ at 500 °C. The response and recovery times to 500 ppb $H_2S$ are 20 s and 58 s, respectively (Fig. 6**(b)**). The dependence relation between ΔV and 0.005–5 ppm $H_2S$ concentrations is divided into two periods below and high than 0.1 ppm, which the linear slop (sensitivity) in the ranges of 0.005–0.1 ppm $H_2S$ and logarithm linear slop (sensitivity) in the ranges of 0.1–5 ppm $H_2S$ is −102 mV/ppm and −67 mV/decade at 500 °C (Fig. 6**(c)**). Comparing with reported state-of-the-art YSZ-based mixed potential type $H_2S$ gas sensors in Table 1, the developed sensor utilizing $ZnMoO_4$-SE sintered at 800 °C displays fast response and recovery times as well as the lowest detection limit to $H_2S$, except for sensitivity. The electrochemical cells and electrode reactions for the developed sensor can be expressed as follows:

In air atmosphere: $O_2$, $ZnMoO_4$/YSZ/Pt, $O_2$ (1)

In $H_2S$ atmosphere: $H_2S + O_2$, $ZnMoO_4$/YSZ/Pt, $H_2S + O_2$ (2)

Cathodic reaction: $O_2 + 4e^- \rightarrow 2O^{2-}$ (3)

Anodic reaction: $H_2S + 3O^{2-} \rightarrow SO_2 + H_2O + 6e$- (4)

The sensing process of the mixed potential type sensing device is attributed to the gas phase heterogeneous catalytic reaction in sensing electrode layer and electrochemical catalytic reaction activity at TPB. When the sensor was exposed to tested gas ($H_2S$), $H_2S$ gas passed through $ZnMoO_4$ sensing electrode layer and arrived at TPB, which occurred electrochemical reactions. Part of $H_2S$ gas is lost in diffusion process due to heterogeneous gas phase catalytic reaction ($2H_2S + 3O_2 \rightarrow 2SO_2 + 2H_2O$). More remarkable, the loose and porous structure of sensing electrode layer will improve passing rate of $H_2S$ and reduce the consumption (Fig. 3**(a)**). This may ensure that more $H_2S$ gas participate in electrochemical reaction process and produce high response signal. The different concentrations of $H_2S$ (air) occurred simultaneously electrochemical reduction (3) and oxidation reaction (4) at TPB of $ZnMoO_4$ sensing electrode and formed local cell. The mixed potential was observed at equilibrium of two electrochemical reaction.

In the higher $H_2S$ tested concentrations (< 0.1 ppm), the mixed potential of the sensor attached with $ZnMoO_4$-SE is dependent on rate-limiting kinetics based on Tafel-type behavior. To gain more insight into this sensing phenomenon, the potential response to $H_2S$ in air for the fabricated sensor can be treated quantitatively depending on the Butler-Volmer equation [31,32]. The cathodic and anodic current for reactions (3) and (4) can be expressed.

$$i_{O_2} = i^0_{O_2} \exp[-4\alpha F(V - V^0_{O_2})/RT] \quad (5)$$

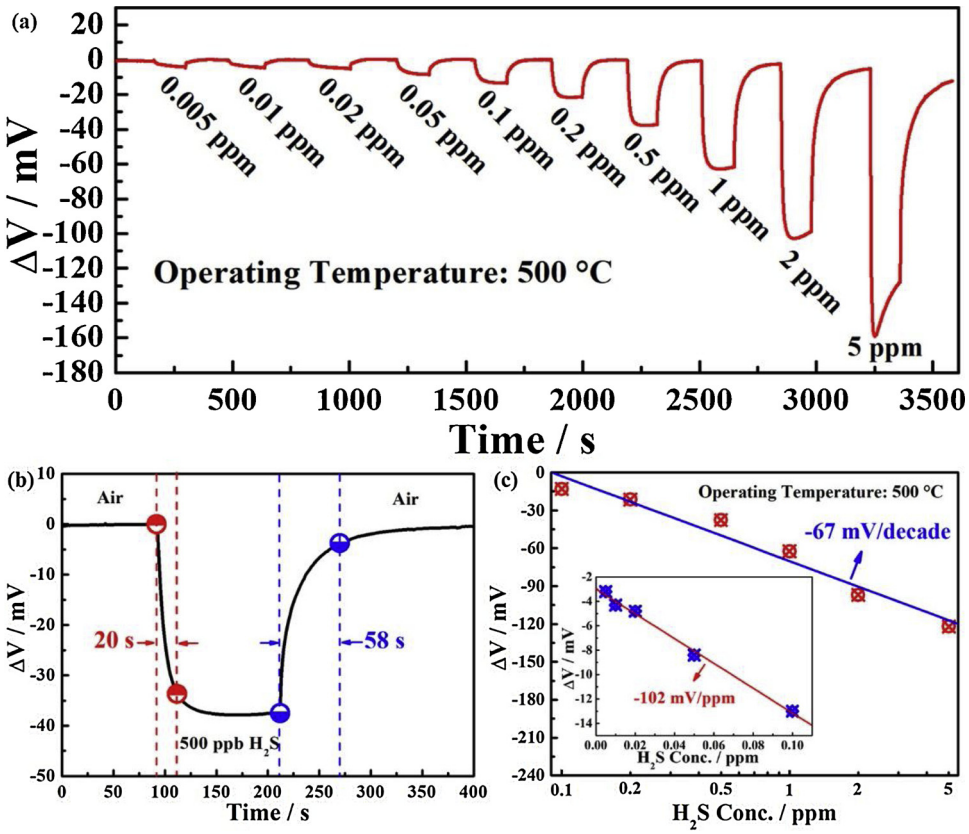


**Fig. 6.** (a) Response transients of the sensor using $ZnMoO_4$-SE sintered at 800 °C to 0.005–5 ppm $H_2S$ at 500 °C; (b) Response and recovery characteristics of the sensor to 500 ppb $H_2S$ at 500 °C; (c) Relation between ΔV and the concentration logarithm of 0.005–5 ppm $H_2S$.

**Table 1**
Summary of $H_2S$ sensing performance in this work and other reported YSZ-based mixed potential type devices.

| Sensing Materials | $H_2S$ Conc. (ppm) | Response (mV)[a] | Sensitivity (mV/decade)[a] | Response/ Recovery time (s) | Low Detection limit (ppb) | Ref. |
|---|---|---|---|---|---|---|
| $ZnMoO_4$ | 0.5 | 37.5 | 67 | 20/58 | 5 | This work |
| Pt | 25 | – | 29 | 5400/- | 1000 | [13] |
| $WO_3$ | 12 | – | 40 | 120-180/ 1200 | 600 | [13] |
| $NiMn_2O_4$ | 0.5 | – | 35/125 | 300/275 | 50 | [19] |
| $La_2NiO_4$ | 0.5 | 55 | 10/69 | 72/1200 | 20 | [20] |

[a] Absolute value.

$$i_{H_2S} = i^0_{H_2S} \exp[6\beta F(V - V^0_{H_2S})/RT] \quad (6)$$

$i^0$: Exchange current density $\alpha$, $\beta$: Transfer coefficient
$F$: Faraday constant $R$: Gas constant $T$: Temperature
$V$ and $V^0$: Electrode potential and the equilibrium electrode potential, respectively $i^0$ is assumed to follow the kinetic equations:

$$i^0_{O_2} = -B_1 C^m_{O_2} \quad (7)$$

$$i^0_{H_2S} = B_2 C^n_{H_2S} \quad (8)$$

Where, $B_1$, $B_2$, $m$ and $n$ are constants; $C$ is gas concentration. The mixed potential $V_M$ under equilibrium state can be presented as follows:

$$V_M = V_0 - nA \ln C_{H_2S} + mA \ln C_{O_2} \quad (9)$$

Here,

$$V_0 = \frac{RT}{(4\alpha + 6\beta)F} \ln \frac{B_1}{B_2} + \frac{2\alpha V^0_{O_2} + 3\beta V^0_{H_2S}}{2\alpha + 3\beta} \quad (10)$$

$$A = \frac{RT}{(4\alpha + 6\beta)F} \quad (11)$$

When $O_2$ concentration is fixed, Eq. (10) is simplified:

$$V_M = V_0 - nA \ln C_{H_2S} \quad (12)$$

Clearly, the negative logarithm linear relationship (-nA) between $V_M$ and $H_2S$ concentration was displayed under constant $O_2$ concentration, in agreement with result experimentally observed in Fig. 6**(c)**.

In the lower $H_2S$ tested concentration (< 0.1 ppm), the diffusion limited kinetic is dominant in the sensing process. A high heterogeneous catalytic oxidation rate on the electrode layer will lower the concentration of $H_2S$ that reaches electrochemical active sites at triple-phase boundary [33,34]. In this regard, the gas diffusion rate in the sensing electrode layer is slower than the electrochemical catalytic oxidation reaction of $H_2S$. The mixed potential $V_M$ yields

$$V_M = V^0_{O_2} - RT \frac{AD_{H_2S} C_{H_2S}}{3B_1 \delta C^m_{O_2}} \quad (13)$$

where A is the electrode area, $D_{H_2S}$ is the diffusion coefficient of $H_2S$ and $\delta$ is the diffusion boundary layer thickness. And the mixed potential presents a negative linear dependence relationship on $H_2S$ concentration, which is consistence with observed result in inset of Fig. 6**(c)**.

For the practical application of gas sensor, the sensing performances, such as good repeated response capability, selectivity, humidity and temperature stability, are crucial and meaningful evaluation parameters for meeting to requirement of actual condition. Fig. 7 depicts the continuous response and recovery characteristics of the sensor utilizing $ZnMoO_4$-SE calcinated at 800 °C to 0.05 ppm and 1 ppm $H_2S$ at 500 °C. Evidently, in the process of the examined seven cycles, the potential signal of the present device in air and 0.05 ppm or 1 ppm $H_2S$ was effectively reproduced, confirming good reproducibility to $H_2S$.

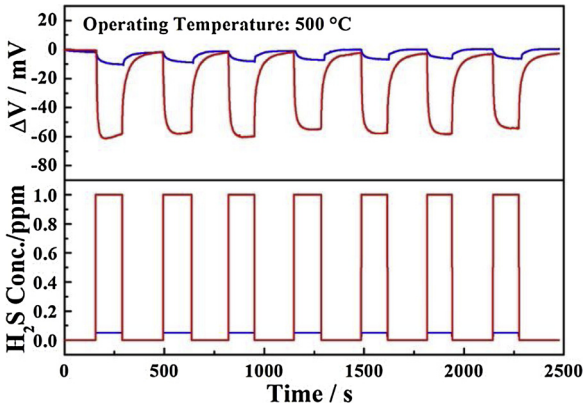


**Fig. 7.** Continuous response and recovery curves of the sensor attached with $ZnMoO_4$-SE sintered at 800 °C to 50 ppb and 1 ppm $H_2S$ at 500 °C.

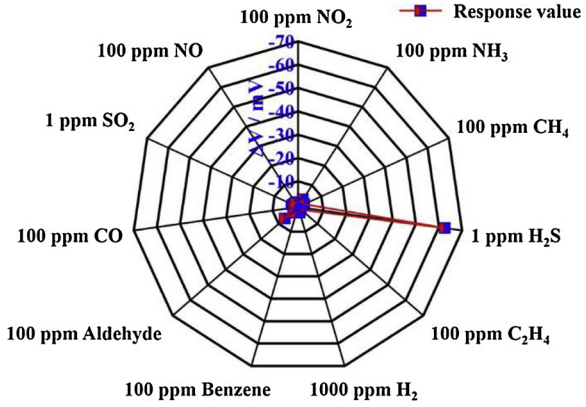


**Fig. 8.** Cross-sensitivities for the sensor using $ZnMoO_4$-SE sintered at 800 °C to various target gases at 500 °C.

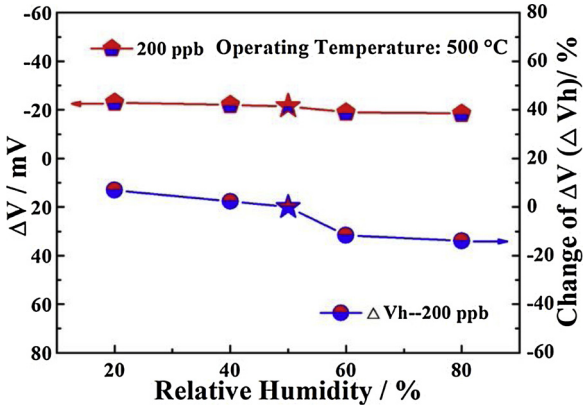


**Fig. 9.** The effect of the different relative humidity on response value for the sensor attached with $ZnMoO_4$-SE sintered at 800 °C at 500 °C.

Subsequently, the responses of the present sensor to various types of gases were investigated at 500 °C and results obtained are summarized in Fig. 8. The response values of the fabricated sensor to 1 ppm $SO_2$, 100 ppm CO, aldehyde, benzene, $C_2H_2$, $CH_4$, $NO_2$, NO, $NH_3$, and 1000 ppm $H_2$ are all less than −7 mV at 500 °C. The response of the present sensor toward 1 ppm $H_2S$ is 9.6–89 times higher than those to other gases, demonstrating the excellent selectivity to $H_2S$ as oppose to any other interfering gases. Meanwhile, the effect of different relative humidity on response value is also investigated and shown in Fig. 9. It can be seen that the response value of the sensor to 200 ppb $H_2S$ in the relative humidity ranges of 20%–80% at 500 °C changed slightly in the extent of -14%-7%, which indicates the relative outstanding resist ability to humidity interference. Furthermore, Fig. 10 shows the high temperature stability of the sensor attached with $ZnMoO_4$-SE sintered at 800 °C to 500 ppb $H_2S$ in 7 days of constant high temperature of 500 °C test periods. For response transients of the present device toward $H_2S$ in the measurement process, times exposed to air and $H_2S$ are kept consistent in each measurement situation and the response exposed to $H_2S$ at last minute as the response value. The response value of the sensor using $ZnMoO_4$-SE sintered at 800 °C to 500 ppb $H_2S$ varied slightly during one week measurement period at 500 °C. The quantitative result demonstrated that the response value change amplitude to 500 ppb $H_2S$ on the 7th day is −6.7%, further illustrating good stability. Overall considering the integral $H_2S$ sensing performance for the developed device, $ZnMoO_4$ is a robust pipeline of new gas sensor using stabilized zirconia solid electrolyte for monitoring $H_2S$ at high temperature.

To certain the sensing mechanism of the developed sensing device involving in the mixed potential model. The polarization curves for the sensor attached with $ZnMoO_4$-SE sintered at 800 °C in air, 0.5 ppm and 1 ppm $H_2S$ were displayed in Fig. 11. The mixed potential can be estimated from the intersection of the cathodic and anodic polarization curves [32,35,36]. It can be obviously seen that the estimated values (−39.5 and −58 mV) for sensors attached with $ZnMoO_4$-SE sintered at 800 °C to 500 ppb and 1 ppm $H_2S$ are approach to those of the response values experimentally observed (-37.5 and -62.5 mV) indicating that the fabricated device obeys to the mixed-potential principle.

## 4. Conclusion

In short, the developed planar stabilized zirconia-based mixed potential type gas sensor utilizing Zinc molybdate ($ZnMoO_4$) as sensing electrode revealed the significant and enormous capacity in the aspect of monitoring rapidly low concentration of $H_2S$ at high temperature. The YSZ-based sensor attached with $ZnMoO_4$-SE sintered at 800 °C exhibited the highest response signal to 1 ppm $H_2S$, comparing with other molybdate electrodes ($NiMoO_4$ and $CoMoO_4$). The present sensor showed the response value of -37.5 mV and -122 mV to 500 ppb $H_2S$ and 5 ppm $H_2S$ at 500 °C, the detection limit of $H_2S$ is even lower to 5 ppb. Between the potential response and $H_2S$ concentration displayed linear relationship in the range of 5–100 ppb and logarithm relationship in the range of 0.1–5 ppm, which the slope is −102 mV/ppm and −67 mV/decade, respectively. The developed sensing device also possessed good reproducibility, stability, selectivity and humidity resistance to $H_2S$. The present investigation is to shine a light on the future development trend of solid electrochemical sensing device based on the mixed potential model for detection of low concentration hazardous gas.

## Acknowledgements

This work is supported by the National Nature Science Foundation of China (Nos. 61831011, 61803171, 61327804, 61520106003, 61722305 and 61833006), Program for Chang Jiang Scholars and Innovative Research Team in University (No. IRT13018), National Key Research and Development Program of China (Nos. 2016YFC0207300 and 2016YFC0201002), Application and Basic Research of Jilin Province (20130102010 JC), Young Elite Scientists Sponsorship Program by CAST (2018QN RC001), Program for JLU Science and Technology Innovative Research Team (JLUSTIRT 2017TD-07), China Postdoctoral Science Foundation Funded Project (No. 2018M630322, 2019T120239), Jilin Provincial Science and Technology Development Program (20190103155JH), Jilin Provincial Education Department Science and Technology Project (JJKH20190114KJ), Fundamental Research Funds for the Central Universities.

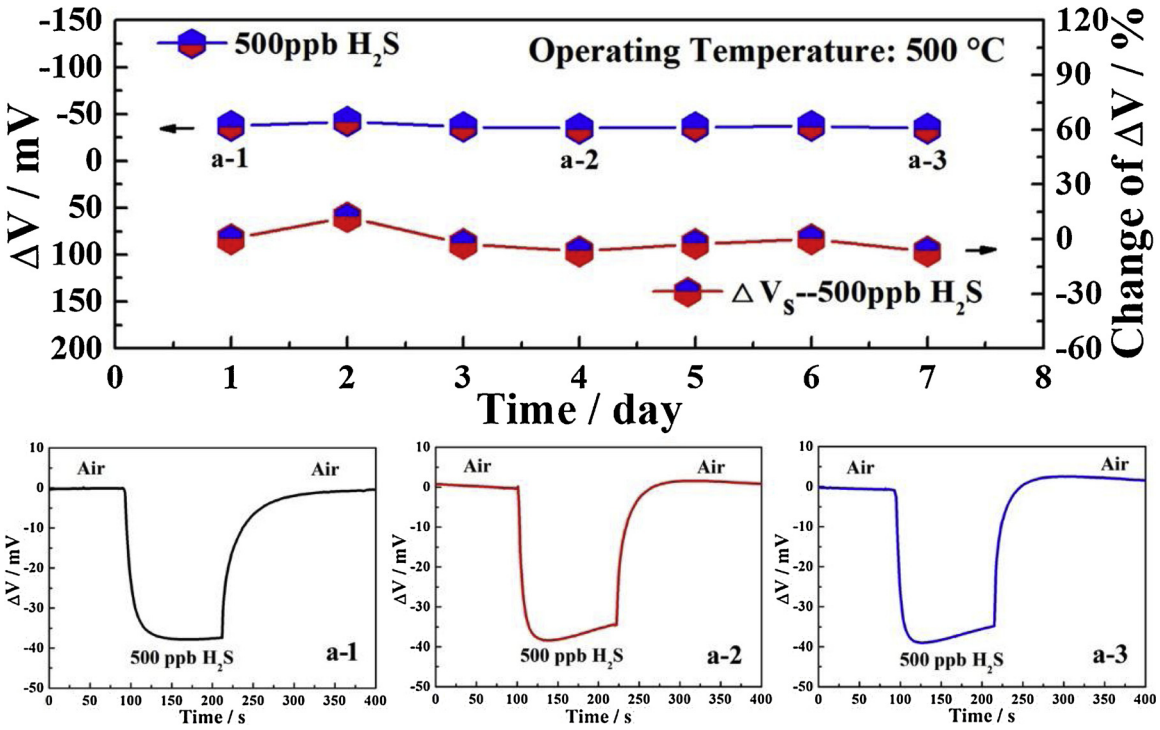


**Fig. 10.** Response variation of the sensor attached with $ZnMoO_4$-SE sintered at 800 °C to 500 ppb $H_2S$ for continuous high temperature operating within one week.

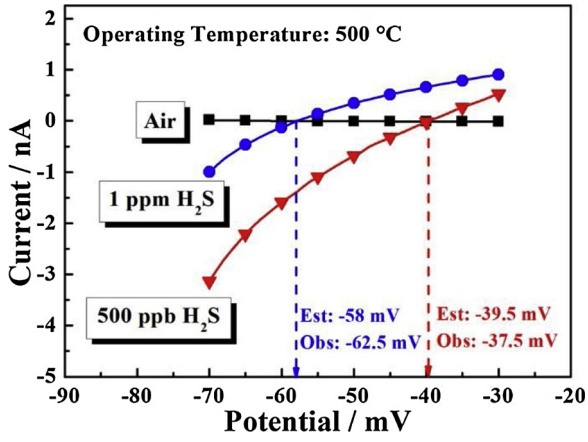


**Fig. 11.** Polarization curves of the sensor attached with $ZnMoO_4$-SE sintered at 800 °C in air, 500 ppb and 1 ppm $H_2S$ at 500 °C.

## References


[1] F. Ali, F. Awwad, Y. Greish, S. Mahmoud, Hydrogen sulfide ($H_2S$) gas sensor: a review, IEEE Sens. J. 19 (2019) 2394–2407.

[2] J.M. Lee, B.U. Moon, C.H. Shim, B.C. Kim, M.B. Lee, D.D. Lee, J.H. Lee, $H_2S$ micro-gas sensor fabricated by thermal oxidation of Cu/Sn double layer, Sens. Actuators B Chem. 108 (2005) 84–88.

[3] Y. Zeng, K. Zhang, X. Wang, Y. Sui, B. Zou, W. Zheng, G. Zou, Rapid and selective $H_2S$ detection of hierarchical $ZnSnO_3$ nanocages, Sens. Actuators B Chem. 159 (2011) 245–250.

[4] R. Ionescu, A. Hoel, C. Granqvist, E. Llobet, P. Heszler, Low-level detection of ethanol and $H_2S$ with temperature-modulated $WO_3$ nanoparticle gas sensors, Sens. Actuators B Chem. 104 (2005) 132–139.

[5] Z.S. Hosseinia, A. Iraji Zad, A. Mortezaali, Room temperature $H_2S$ gas sensor based on rather aligned ZnO nanorods with flower-like structures, Sens. Actuators B Chem. 207 (2015) 865–871.

[6] S.T. Navale, C. Liu, P.S. Gaikar, V.B. Patil, R.U.R. Sagar, B. Du, R.S. Manee, F.J. Stadler, Solution-processed rapid synthesis strategy of $Co_3O_4$ for the sensitive and selective detection of $H_2S$, Sens. Actuators B Chem. 245 (2017) 524–532.

[7] L. Guo, N. Xie, C. Wang, X. Kou, M. Ding, H. Zhang, Y. Sun, H. Song, Y. Wang, G. Lu, Enhanced hydrogen sulfide sensing properties of Pt-functionalized α-$Fe_2O_3$ nanowires prepared by one-step electrospinning, Sens. Actuators B Chem. 255 (2018) 1015–1023.

[8] C. Han, X. Li, C. Shao, X. Li, J. Ma, X. Zhang, Y. Liu, Composition-controllable p-CuO/n-ZnO hollow nanofibers for high-performance $H_2S$ detection, Sens. Actuators B Chem. 285 (2019) 495–503.

[9] F. Zhang, Y. Xu, X. Zhang, L. Sui, P. Hu, Z. Zheng, X. Cheng, S. Gao, H. Zhao, L. Huo, Highly selective ppb-level $H_2S$ sensor based on the walnut-like $Bi_2MoO_6$ at low temperature, Sens. Actuators B Chem. 277 (2018) 312–319.

[10] G.N. Chaudhari, M. Alvi, H.G. Wankhade, A.B. Bodade, S.V. Manorama, Nanocrystalline chemically modified $CdIn_2O_4$ thick films for $H_2S$ gas sensor, Thin Solid Films 520 (2012) 4057–4062.

[11] X. Liang, Y. He, F. Liu, B. Wang, T. Zhong, B. Quan, G. Lu, Solid-state potentiometric $H_2S$ sensor combining NASICON with $Pr_6O_{11}$-doped $SnO_2$ electrode, Sens. Actuators B Chem. 125 (2007) 544–549.

[12] X. Yang, Y. Zhang, X. Hao, Y. Song, X. Liang, F. Liu, F. Liu, P. Sun, Y. Gao, X. Yan, G. Lu, Nafion-based amperometric $H_2S$ sensor using Pt-Rh/C sensing electrode, Sens. Actuators B Chem. 273 (2018) 635–641.

[13] N. Miura, Y. Yan, G. Lu, N. Yamazoe, Sensing characteristics and mechanism of hydrogen sulfide sensor using stabilized zirconia and oxide sensing electrode, Sens. Actuators B Chem. 34 (1996) 367–372.

[14] A.F. Abu-Hani, Y.E. Greish, S.T. Mahmoud, F. Awwad, A.I. Ayesh, Low-temperature and fast response $H_2S$ gas sensor using semiconducting chitosan film, Sens. Actuators B Chem. 253 (2017) 677–684.

[15] J. Shu, Z. Qiu, S. Lv, K. Zhang, D. Tang, Cu2+-doped SnO2 nanograin/ polypyrrole nanospheres with synergic enhanced properties for ultrasensitive room-temperature $H_2S$ gas sensing, Anal. Chem. 89 (2017) 11135–11142.

[16] L. Guo, M. Wang, D. Cao, A novel Zr-MOF as fluorescence turn-on probe for real-time detecting $H_2S$ gas and fingerprint identification, Small 14 (2018) 1703822.

[17] X. Dong, Y. Su, T. Lu, L. Zhang, L. Wu, Y. Lv, MOFs-derived dodecahedra porous $Co_3O_4$: an efficient cataluminescence sensing material for $H_2S$, Sens. Actuators B Chem. 258 (2018) 349–357.

[18] H. Zhang, T. Zhong, R. Sun, X. Liang, G. Lu, Sub-ppm $H_2S$ sensor based on NASICON and $CoCr_{2-x}Mn_xO_4$ sensing electrode, RSC Adv. 4 (2014) 55334–55340.

[19] Y. Guan, C. Yin, X. Cheng, X. Liang, Q. Diao, H. Zhang, G. Lu, Sub-ppm $H_2S$ sensor based on YSZ and hollow balls $NiMn_2O_4$ sensing electrode, Sens. Actuators B Chem. 193 (2014) 501–508.

[20] X. Hao, C. Ma, X. Yang, T. Liu, B. Wang, F. Liu, X. Liang, C. Yang, H. Zhu, G. Lu, YSZ-based mixed potential $H_2S$ sensor using $La_2NiO_4$ sensing electrode, Sens. Actuators B Chem. 255 (2018) 3033–3039.

[21] F. Liu, J. He, Z. Yang, R. You, J. Wang, L. Zhao, Q. Wang, X. Liang, P. Sun, X. Yan, G. Lu, The mixed potential type gas sensor based on stabilized zirconia and molybdate $MMoO_4$ (M: Ni, Co and Zn) sensing electrode aiming at detecting triethylamine, Sens. Actuators B Chem. 267 (2018) 430–437.

[22] S.C. Abrahams, Crystal structure of the transition-metal molybdates and tungstates. III. dismagnetic α-$ZnMoO_4$, J. Chem. Phys. 46 (1967) 2052–2063.

[23] L. Aleksandrov, T. Komatsu, R. Iordanova, Y. Dimitriev, Structure study of $MoO_3$-ZnO-$B_2O_3$ glasses by Raman spectroscopy and formation of α-$ZnMoO_4$ nanocrystals, Opt. Mater. 33 (2011) 839–845.

[24] Y. Liang, P. Liu, H.B. Li, G.W. Yang, $ZnMoO_4$ micro- and nanostructures synthesized by electrochemistry-assisted laser ablation in liquids and their optical properties,

Cryst. Growth Des. 12 (2012) 4487–4493.
[25] D.C. Agarwal, D.K. Avasthi, S. Varma, F. Kremer, M.C. Ridgway, D. Kabiraj, Phase transformation of $ZnMoO_4$ by localized thermal spike, J. Appl. Phys. 115 (2014) 163506(1-5).
[26] Y.-P. Gao, K.-J. Huang, C.-X. Zhang, S.-S. Song, X. Wu, High-performance symmetric supercapacitor based on flower-like zinc molybdate, J. Alloys. Compd. 731 (2018) 1151–1158.
[27] G.K. Veerasubramani, K. Krishnamoorthy, S.J. Kim, Improved electrochemical performances of binder-free $CoMoO_4$ nanoplate arrays@Ni foam electrode using redox additive electrolyte, J. Power Sources 306 (2016) 378–386.
[28] F. Liu, B. Wang, X. Yang, Y. Guan, R. Sun, Q. Wang, X. Liang, P. Sun, G. Lu, High-temperature stabilized zirconia-based sensors utilizing $MNb_2O_6$ (M: Co, Ni and Zn) sensing electrodes for detection of $NO_2$, Sens. Actuators B Chem. 232 (2016) 523–530.
[29] K. Mahendraprabhu, A.S. Sharma, P. Elumalai, CO sensing performances of YSZ-based sensor attached with sol-gel derived ZnO nanospheres, Sens. Actuators B Chem. 283 (2019) 842–847.
[30] A. Bhardwaj, I.H. Kim, J.W. Hong, A. Kumar, S.J. Song, Transition metal oxide (Ni, Co, Fe)-tin oxide nanocomposite sensing electrodes for a mixed-potential based $NO_2$ sensor, Sens. Actuators B Chem. 284 (2019) 534–544.
[31] F.H. Garzon, R. Mukundan, E.L. Brosha, Solid-state mixed potential gas sensors: theory, experiments and challenges, Solid State Ion. 136-137 (2000) 633–638.
[32] N. Miura, T. Sato, S.A. Anggraini, H. Ikeda, S. Zhuiykov, A review of mixed-potential type zirconia-based gas sensors, Ionics 20 (2014) 901–925.
[33] H. Zhang, J. Yi, X. Jiang, Fast response, highly sensitive and selective mixed-potential $H_2$ sensor based on (La, Sr)(Cr, Fe)$O_{3-\delta}$ perovskite sensing electrode, ACS Appl. Mater. Interfaces 9 (2017) 17218–17225.
[34] X. Zhang, H. Kohler, M. Schwotzer, Y.H. Wu, U. Guth, Mixed-potential gas sensor with layered Au, Pt-YSZ electrode: investigating the sensing mechanism with steady state and dynamic electrochemical methods, Sens. Actuators B Chem. 252 (2017) 554–560.
[35] H. Jin, X. Zhang, C. Hua, X. Zhang, J. Zou, W. Shen, J. Jian, Further enhancement of the light-regulated mixed-potential signal with ZnO-based electrodes, Sens. Actuators B Chem. 255 (2018) 3516–3522.
[36] R. You, X. Hao, H. Yu, B. Wang, G. Lu, F. Liu, T. Cui, High performance mixed-potential-type zirconia-based $NO_2$ sensor with self-organizing surface structure fabricated by low energy ion beam etching, Sens. Actuators B Chem. 263 (2018) 445–451.

**Fangmeng Liu** received his PhD degree in 2017 from College of Electronic Science and Engineering, Jilin University, China. Now he is a lecturer of Jilin University, China. His current research interests include the application of functional materials and development of solid state electrochemical gas sensor and flexible device.

**Jing Wang** received her B.S. degree in applied chemistry in 2009 and the M.S. degree in polymer chemistry and physics in 2012 from Northeast Forestry University in China. Now, she is studying for her Ph.D. degree in College of Electronic Science and Engineering, Jilin University, China.

**Rui You** received his B.S. degree from Department of Opto-Electronic Engineering in 2013, Changchun University of Science and Technology, Changchun, China. He is now a Ph.D. student at the Department of Precision Instrument at Tsinghua University, Beijing, China. Currently his research interests mainly include gas sensor and application of MEMS process.

**Zijie Yang** received the B.S. degree in department of electronic science and technology in 2017. He is currently studying for his M.E. Sci. degree in College of Electronic Science and Engineering, Jilin University, China.

**Junming He** received the B.Eng. degree in department of electronic science and technology in 2017. She is currently studying for her M.E. Sci. degree in College of Electronic Science and Engineering, Jilin University, China.

**Caileng Wang** received the B.S. degree in department of microelectronics science and engineering in 2018. She is currently studying for her M.E. Sci. degree in College of Electronic Science and Engineering, Jilin University, China.

**Ao Liu** received the B.S. degree in department of electronic science and technology in 2018. He is currently studying for his M.E. Sci. degree in College of Electronic Science and Engineering, Jilin University, China.

**Qingji Wang** received the B.Eng. degree in electronic and information engineering from Beijing University of Chemical Technology in 2007. Now he is a lecturer of Hainan University, China.

**Xu Yan** received his M.S. degree in 2013 from Nanjing Agricultural University. He joined the group of Prof. Xingguang Su at Jilin University and received his Ph.D. degree in June 2017. Since then, he did postdoctoral work with Prof. Geyu Lu. Currently, his research interests mainly focus on the development of the functional nanomaterials for chem/bio sensors.

**Peng Sun** received his PhD degree from the Electronics Science and Engineering department, Jilin University, China in 2014. Now, he is engaged in the synthesis and characterization of the semiconducting functional materials and gas sensors.

**Geyu Lu** received the B.Sci. degree in electronic sciences in 1985 and the M.S. degree in 1988 from Jilin University in China and the Dr. Eng. degree in 1998 from Kyushu University in Japan. Now he is a professor of Jilin University, China. His current research interests include the development of chemical sensors and the application of the function materials.